Original Article | Experimental and Others

http://dx.doi.org/10.3348/kjr.2016.17.1.83
pISSN 1229-6929 · eISSN 2005-8330
Korean J Radiol 2016;17(1):83-92

Korean Journal of Radiology
KJR

Coronary Microembolization with Normal Epicardial Coronary Arteries and No Visible Infarcts on Nitrobluetetrazolium Chloride-Stained Specimens: Evaluation with Cardiac Magnetic Resonance Imaging in a Swine Model

Hang Jin, MD, PhD[1, 2], Hong Yun, MD, PhD[1, 2], Jianying Ma, MD, PhD[3], Zhangwei Chen, MD, PhD[3], Shufu Chang, MD, PhD[3], Mengsu Zeng, MD, PhD[1, 2]

[1]Department of Radiology, Zhongshan Hospital, Fudan University and Shanghai Institute of Medical Imaging, Shanghai 200032, China; [2]Department of Medical Imaging, Shanghai Medical College, Fudan University, Shanghai 200032, China; [3]Department of Cardiology, Zhongshan Hospital, Fudan University and Shanghai Institute of Cardiovascular Diseases, Shanghai 200032, China

Objective: To assess magnetic resonance imaging (MRI) features of coronary microembolization in a swine model induced by small-sized microemboli, which may cause microinfarcts invisible to the naked eye.

Materials and Methods: Eleven pigs underwent intracoronary injection of small-sized microspheres (42 μm) and catheter coronary angiography was obtained before and after microembolization. Cardiac MRI and measurement of cardiac troponin T (cTnT) were performed at baseline, 6 hours, and 1 week after microembolization. Postmortem evaluation was performed after completion of the imaging studies.

Results: Coronary angiography pre- and post-microembolization revealed normal epicardial coronary arteries. Systolic wall thickening of the microembolized regions decreased significantly from 42.6 ± 2.0% at baseline to 20.3 ± 2.3% at 6 hours and 31.5 ± 2.1% at 1 week after coronary microembolization ($p < 0.001$ for both). First-pass perfusion defect was visualized at 6 hours but the extent was largely decreased at 1 week. Delayed contrast enhancement MRI (DE-MRI) demonstrated hyperenhancement within the target area at 6 hours but not at 1 week. The microinfarcts on gross specimen stained with nitrobluetetrazolium chloride were invisible to the naked eye and only detectable microscopically. Increased cTnT was observed at 6 hours and 1 week after microembolization.

Conclusion: Coronary microembolization induced by a certain load of small-sized microemboli may result in microinfarcts invisible to the naked eye with normal epicardial coronary arteries. MRI features of myocardial impairment secondary to such microembolization include the decline in left ventricular function and myocardial perfusion at cine and first-pass perfusion imaging, and transient hyperenhancement at DE-MRI.

Index terms: *Coronary angiography; Cardiac MR imaging; Myocardial contraction; Myocardial microinfarct*

Received April 14, 2015; accepted after revision October 15, 2015.
This work was supported by the National Natural Science Foundation of China (Grant Number 81201070 to H.J. and 81200146 to Z.W.C.) and Fudan University Foundation for young teachers to improve scientific research ability (Grant Number 20520133486 to H.J.).
Corresponding author: Mengsu Zeng, MD, PhD, Department of Radiology, Zhongshan Hospital, Fudan University, 180#, Feng Lin Road, Shanghai 200032, China.
• Tel: (8621) 64041990 • Fax: (8621) 64038472 • E-mail: zeng.mengsu@hotmail.com

INTRODUCTION

Coronary microembolization secondary to atherosclerotic plaque rupture occurs clinically in ischemic heart disease, spontaneously in patients with unstable angina or acute coronary syndromes (1-3), as well as artificially during coronary interventions (4-6). The pathophysiological significance and typical consequences include perfusion-contraction mismatch, notable arrhythmias, myocardial ischemia, microinfarction, and contractile dysfunction (7-9). Several noninvasive methods are developed to aid in the detection of microvascular obstruction, including positron emission tomography, contrast material-enhanced echocardiography and contrast-enhanced magnetic resonance (MR) imaging (10-14). MR imaging (MRI) permits an integrated examination of cardiac morphology and function, myocardial perfusion, myocardial viability and coronary artery anatomy (15-19). Several reports indicate the usefulness of first-pass perfusion and delayed contrast enhancement, as well as serial MR imaging, for the assessment of effects of microembolization created with intracoronary injection of relatively large embolic agents that lead to visually detectable myocardial microinfarcts on gross specimen (20-23). However, the effects of microembolization may be related to the size of embolized microvessels (20-26). Furthermore, small-sized microemboli, which may escape the protective devices placed distal to atherosclerotic lesions during percutaneous coronary interventions, may cause myocardial infarcts invisible on gross specimen. We aimed to evaluate the acute and subacute effects of coronary microembolization in a swine model induced by small-sized microemboli using cardiac MR imaging. In addition, evaluation of coronary angiography after microembolization in animal studies is rarely reported (20-23, 25, 26); hence, we aimed to assess the immediate effect of microembolization on coronary arteries with coronary angiography pre- and post-microembolization.

MATERIALS AND METHODS

Experimental Preparation and Protocols

All experimental protocols were approved by the institutional committee on animal research, and the study was performed in accordance with the Guide for the Care and Use of Laboratory Animals (NIH Publication No. 85–23, Revised 1996). Twelve pigs (23.2 ± 1.5 kg) were premedicated with a combination of ketamine (5–10 mg/kg) and diazepam (5–10 mg/kg). Anesthesia was induced and maintained by 3% pentobarbital sodium intravenously. Anticoagulation was induced with an intravenous bolus injection of 5000 IU heparin sodium, and additional doses of 100 IU/kg heparin sodium per hour were given to maintain heparinization. After establishing femoral artery access, coronary angiography of the left coronary artery was performed with a 6-Fr XB 3.5 guiding catheter. A 2.8-Fr infusion catheter (Cordis Inc., Johnson & Johnson, New Brunswick, NJ, USA) was deployed in the left anterior descending coronary artery (LAD) distal to the second diagonal branch. One pig died during coronary catheterization because of ventricular fibrillation. Microembolization was created with slow injection of 120000 microspheres (42 μm Dynospheres; Dyno Particles; Lillestrøm, Norway) through the coronary catheter. After the delivery of the embolic agent, coronary angiography was performed repeatedly in order to assess the immediate effect of microembolization on coronary arteries. Cine-angiograms were evaluated off line by consensus of 2 cardiologists with no microembolization status provided on the images.

MR Imaging

MR examinations were performed on a 1.5T MR imaging unit (Magnetom Avanto; Siemens Medical Solutions, Erlangen, Germany) equipped with high-performance gradients (maximum strength, 45 mT/m; slew rate, 200 T/m/s) and a phased-array total imaging matrix coil. Six (anterior/posterior) coil elements positioned close to the heart were activated for signal reception. Cardiac MRI protocol and parameters in the current study were based on previous study on microembolization in the swine model and coronary microcirculatory impairment in patients (20, 21, 26, 27) as well as our previous experience in cardiac MR imaging. MRI was carried out before (baseline), 6 hours (acute), and 1 week (subacute) after the selective injection of the microspheres. Scout images were obtained to determine the exact position and standard orientations–long-axis, four-chamber, and short-axis views of the left ventricle.

Cine MR images encompassing the whole left ventricle (LV) in the short-axis view for quantification of regional function, were obtained by using a steady-state free precession sequence applied along with parallel imaging technique i.e., repetition time (TR)/echo time (TE), 2.6/1.3 ms; flip angle, 80°; slice thickness, 8 mm; field of view, 34

Korean Journal of Radiology
KJR

x 26 cm; matrix size, 192 x 154, 20 cardiac phases.

First-pass perfusion MRI was performed to detect the hypoperfused region using an intravenous injection of 0.05 mmol/kg gadolinium-based contrast material (Gd-DTPA, [Magnevist], Bayer Healthcare, Berlin, Germany) in 4 short-axis slices spaced to encompass the microembolized territory. The images were registered using anatomical landmarks such as the anterior right ventricular and papillary muscle insertion points, as well as the distance measurements from the apex. The contrast material was delivered by a power injector at 3 mL/s followed by 10–15 mL saline. First-pass perfusion MR images were acquired using a saturation-recovery gradient-echo sequence, and imaging parameters were as follows: TR/TE, 2.4/1.1 ms; flip angle, 12°; slice thickness, 10 mm; field of view, 34 x 26 cm; matrix size, 192 x 126; acquisition time, 2 R-R intervals per dynamic acquisition.

Delayed contrast enhancement magnetic resonance imaging (DE-MRI) was performed 10 minutes after intravenous injection of an additional 0.15 mmol/kg Gd-DTPA in short-axis views covering the entire LV with a segmented T1-weighted inversion-recovery spoiled gradient-echo sequence. The imaging parameters were as follows: TR/TE, 7.6/3.4 ms; flip angle, 25°; slice thickness, 5 mm; field of view, 34 x 26 cm; matrix size, 256 x 192. The optimal inversion time (TI) to null the signal of normal myocardium was determined by using an inversion-recovery steady-state free precession sequence. Phase-sensitive reconstruction method may reduce the variation in apparent infarct size that is observed in the magnitude images as TI is changed (28); hence, DE-MRI pulse sequence uses both magnitude and phase-sensitive reconstruction to generate 2 images per slice representing the magnitude and phase-sensitive component, respectively.

MR Image Analysis

MR images were reviewed and analyzed in a blinded and random fashion using Argus software on an independent workstation (Leonardo; Siemens Medical Solutions) and Segment, version 1.8, software (29). The visual assessments (presence vs. absence) of myocardial contractile dysfunction, perfusion defect and delayed-enhancement were performed independently by 2 radiologists. The disagreement was settled by a consensus reading.

Systolic wall thickening was analysed using 3 short-axis slices of cine MRI distal to LAD microembolization (8 mm slice thickness, starting at 16 mm from the apex) from each animal at baseline, 6 hours and 1 week after microembolization. Each LV slice was divided into 8 circumferential segments 45° apart with segment 1 beginning at the posterior insertion of the right ventricle and the numbering of the remaining 7 segments proceeding in a clockwise fashion (21). The observers were requested to exclude the papillary muscles during semi-automatic tracing of the endocardium contour for systolic wall thickening analysis. Semiautomatic regional systolic wall thickening was quantified in 8 segments of each slice by using the software. The averages of microembolized (segments 2–5) and remote (segments 1, 6–8) myocardium systolic wall thickening values, derived from 3 short-axis sections were used for statistical analysis. Cine images were also used to calculate the ejection fraction (EF) by delineation of the endocardium on all short-axis images at end diastole and end systole.

The first-pass MR perfusion images obtained at the baseline, 6 hours, and 1 week after microembolization were pooled and randomized, with no time-point information provided on the images. These were subsequently presented to the 2 radiologists for visual analysis. Semi-quantitative parameters of perfusion, namely max upslope, peak signal intensity (SI) and time to peak were determined in the LV blood pool and LAD territory using first-pass perfusion images at the baseline, 6 hours, and 1 week after microembolization. DE-MR images obtained at 6 hours and 1 week after microembolization were evaluated visually by 2 radiologists independently in a blinded and random fashion and the disagreement was settled by consensus of the 2 readers.

Measurement of Cardiac Troponin T (cTnT)

Blood samples were taken at baseline, 6 hours, and 1 week after microembolization. The serum level of cardiac troponin T (cTnT) was quantitatively measured by electrochemiluminescence.

Histopathology

After completion of the MRI examinations, the animals were euthanized with 40 mL of saturated potassium chloride solution. The hearts were excised rapidly, cut into 10-mm-thick slices parallel to the plane of the atrioventricular groove, and soaked for up to 20 minutes in 1.0% nitrobluetetrazolium chloride (NBT) to detect microinfarcts. Representative tissue samples were obtained from the microembolized and remote regions for histopathologic

analysis. The samples were dehydrated and embedded in paraffin in accordance with the standard procedure, sliced into 5-μm slices, and stained with hematoxylin-eosin (HE) for microscopic analysis.

Statistical Analysis

All continuous variables were presented as means ± standard deviation. Eleven animals were used for statistical analysis. The interobserver agreement of the visual evaluation (presence vs. absence) of perfusion defect, myocardial contractile dysfunction and delayed-enhancement between 2 radiologists was performed using Cohen's kappa coefficient, and kappa values were interpreted using a commonly cited scale (30). Values of 0.81–0.99 indicated almost perfect agreement; 0.61–0.80, substantial agreement; 0.41–0.60, moderate agreement; 0.21–0.40, fair agreement; and 0.01–0.20, slight agreement. Comparisons of systolic wall thickening, the semi-quantitative perfusion parameters (max upslope, time to peak and peak enhancement) and the serum level of cTnT between time points were performed with repeated measures analysis of variance followed by the post-hoc test using the least significant difference (LSD) method. A p value < 0.05 was considered significant.

RESULTS

Coronary Angiography

Coronary angiography pre- and post-microembolization showed normal-appearing epicardial arteries. Coronary flow of the Thrombolysis In Myocardial Infarction grade 3 remained in all animals after the administration of microspheres (Fig. 1). All the side branches were well visualized and no occlusion was observed after microembolization.

Myocardial and Global LV Function

Six hours after delivery of the embolic agent, a significant decline in the systolic wall thickening was observed in the embolized territory and quantitative analysis further demonstrated the myocardial dysfunction (baseline, 42.6 ± 2.0% vs. 6 hours, 20.3 ± 2.3%; p < 0.001). At 1 week, myocardial contraction improved partially (1 week, 31.5 ± 2.1% vs. 6 hours, 20.3 ± 2.3%; p < 0.001) but did not recover to basal values in the embolized region (baseline, 42.6 ± 2.0% vs. 1 week, 31.5 ± 2.1%; p < 0.001). The systolic wall thickening of remote myocardium decreased significantly at 6 hours after delivery of the embolic agent (baseline, 44.9 ± 2.2% vs. 6 hours, 35.8 ± 1.9%; p < 0.001), but recovered completely at 1 week (1 week, 43.8 ± 2.5% vs. 6 hours, 35.8 ± 1.9%; p < 0.001 and baseline, 44.9 ± 2.2%; p = 0.132). Details were summarized in Table 1. The LVEF declined from 52 ± 4% at baseline to 35 ± 4% at 6 hours (p < 0.001) and recovered partially to 44 ± 3% at 1 week (p < 0.001 for both the comparison to baseline and 6 hours) after microembolization. Interobserver agreement was excellent (κ = 0.812) for the visual analysis of cine MR images.

Myocardial Perfusion and DE-MR imaging

First-pass perfusion imaging showed perfusion defect within the embolized territory at 6 hours, but the extent of perfusion defect was largely decreased at 1 week. At 6 hours, the maximum SI in the LAD coronary artery territory was lower (552 ± 59) in comparison with the baseline (750 ± 56; p < 0.001), the maximum upslope was lower (6 hours, 102 ± 23 s^{-1} vs. baseline, 157 ± 26 s^{-1}; p < 0.001) and the time to peak was longer (6 hours, 18.3 ± 1.8 seconds vs. baseline, 11.6 ± 0.8 seconds; p < 0.001). At 1 week after microembolization, all the MR perfusion parameters improved, as compared with those at 6 hours (p < 0.05 for all the comparisons). MR estimates of perfusion in the LAD territory differed between the baseline and 1 week after microembolization for maximum upslope (1 week, 141 ± 29 s^{-1} vs. baseline, 157 ± 26 s^{-1}; p = 0.004) and time to peak (1 week, 13.8 ± 1.1 seconds vs. baseline, 11.6 ± 0.8 seconds; p = 0.001) but not for the maximum SI (1 week, 742 ± 66 vs. baseline, 750 ± 56; p = 0.728). Maximum SI, time to peak, and peak slope were not significantly different between 3 time-points (the baseline, 6 hours, and 1 week after microembolization) in the blood pool (p > 0.05 for all). Patchy hyperenhanced regions were visualized on DE-MRI in all animals at 6 hours after microembolization. Hyperenhancement from microembolization at early acute phase was distributed within the transmural extent of the targeted myocardium, rather than confined to the subendocardium region. However, hyperenhanced regions could hardly be observed visually on DE-MRI at 1 week. Semi-quantitative perfusion parameters were listed in Table 2 and the examples of the MR perfusion and DE images were shown in Figure 2A-D. Interobserver agreement was excellent (κ = 0.864) for the evaluation of DE-MRI and substantial (κ = 0.756) for the assessment of MR perfusion images.

Korean Journal of Radiology
KJR

The Serum Level of cTnT

The serum level of cTnT was obtained in 8 of 11 pigs and significantly increased at 6 hours after coronary microembolization (baseline, < 0.01 ng/mL vs. 6 hours, 0.481 ± 0.194 ng/mL; $p < 0.001$). It was still higher at 1 week (0.181 ± 0.161 ng/mL), as compared to baseline ($p = 0.02$). The serum level of cTnT was set as 0.01 ng/mL at baseline, for statistical analyses.

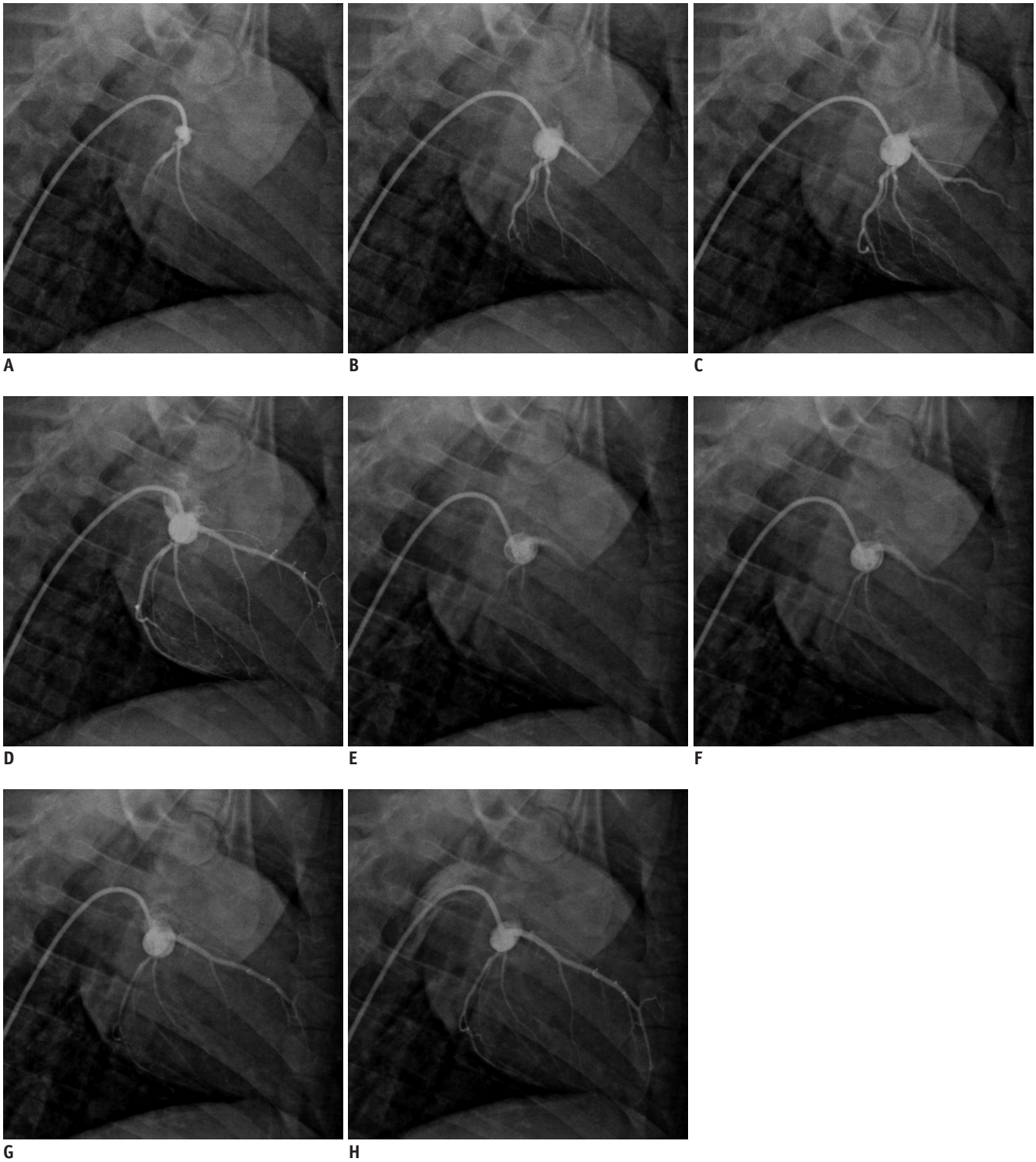

Fig. 1. Coronary angiograms pre- and post-coronary microembolization.
Coronary angiography before **(A-D)** and after coronary microembolization **(E-H)** demonstrates normal-appearing epicardial arteries with coronary flow of TIMI grade 3 after injection of microspheres. TIMI = Thrombolysis In Myocardial Infarction

Histopathologic Results

At 1 week after microembolization, the microinfarcts were invisible to the naked eye on gross NBT specimen in all animals. However, microscopic examination demonstrated the embolic agent in coronary arterioles and the patchy microinfarcts in the embolized areas. The remote myocardium appeared histologically normal. Examples of NBT and HE staining images were shown in Figures 2E and 3.

DISCUSSION

The major findings of the current study can be summarized as follows: a certain load of small-sized microemboli, which may escape the distal protective devices during percutaneous coronary interventions, may cause normal-appearing epicardial coronary arteries on coronary angiography and result in myocardial infarcts invisible to the naked eye; even small-sized microemboli can cause a persistent decline in the systolic wall thickening of the embolized region; first-pass myocardial perfusion MRI can demonstrate acute myocardial ischemia after microembolization; small-sized microemboli may cause regional hyperenhancement of the target area on DE-MRI at 6 hours, but not 1 week; regional assessment of myocardial contractility and perfusion by cine and first-pass perfusion MRI may be better than DE-MRI in the evaluation of the ischemic cascade due to coronary microembolization.

In the current study, DE-MRI revealed hyperenhancement within the target areas at 6 hours after coronary microembolization, but the hyperenhancement disappeared at 1 week. There was no evidence of myocardial infarction on gross NBT specimen at 1 week after microembolization; however, the results of cTnT supported the diagnosis of myocardial infarction in the current study. Several previous MRI studies (20-23) on coronary microembolization using relatively large microemboli, such as 100–300 μm and a mean of 80 μm diameter of 40–120 μm microemboli, have reported hyperenhancement areas on DE-MRI at 1 week and 7–8 weeks and the myocardial microinfarcts could be detected visually on gross specimen using TTC. However, it is likely that different definitions of microinfarcts were used. Pathologists have used the term microinfarcts for microscopically detectable myocardial necrosis but not for infarcts visually detectable on gross specimen, and the term heterogeneous infarcts for areas of non-uniform early myocardial necrosis and scar (3). Previous MRI studies (20-23, 25) with relatively large microemboli have used the term microinfarcts for heterogeneous and multifocal small areas of infarcts within the territory undergoing microembolization and the infarction could be observed on gross specimen. In the current study, the microinfarcts due to a certain load of small-sized microemboli (42 μm) were undetectable visually on gross specimen at 1 week. Thus, visualization of such microinfarcts directly with DE-MRI could be challenging, due to the very small areas of myocardial infarction, inadequate brightness because

Table 1. Regional Assessment of Left Ventricular Systolic Wall Thickening before and after Coronary Microembolization

	LAD Territory	Remote Myocardium
Baseline (%)	42.6 ± 2.0*‡	44.9 ± 2.2*
6 hours (%)	20.3 ± 2.3*†	35.8 ± 1.9*†
1 week (%)	31.5 ± 2.1†‡	43.8 ± 2.5†

All data are expressed as means ± SD. *p < 0.05 for comparison of baseline to 6 hours, †p < 0.05 for comparison of 6 hours to 1 week, ‡p < 0.05 for comparison of 1 week to baseline. LAD = left anterior descending artery, SD = standard deviation

Table 2. Regional Assessment of Myocardial Perfusion before and after Coronary Microembolization

Parameters	Maximum Upslope (sec^{-1})	Maximum Signal Intensity	Time to Peak (sec)
Before microembolization			
LV blood	588 ± 55	2140 ± 321	5.8 ± 0.5
LAD territory	157 ± 26*‡	750 ± 56*	11.6 ± 0.8*‡
6 hours after microembolization			
LV blood	618 ± 68	2228 ± 294	5.5 ± 0.4
LAD territory	102 ± 23*†	552 ± 59*†	18.3 ± 1.8*†
1 week after microembolization			
LV blood	607 ± 71	2133 ± 232	5.6 ± 0.4
LAD territory	141 ± 29†‡	742 ± 66†	13.8 ± 1.1†‡

All data are expressed as means ± SD. *p < 0.05 for comparison of baseline to 6 hours, †p < 0.05 for comparison of 6 hours to 1 week, ‡p < 0.05 for comparison of 1 week to baseline. LAD = left anterior descending artery, LV = left ventricle, SD = standard deviation

Korean Journal of Radiology
KJR

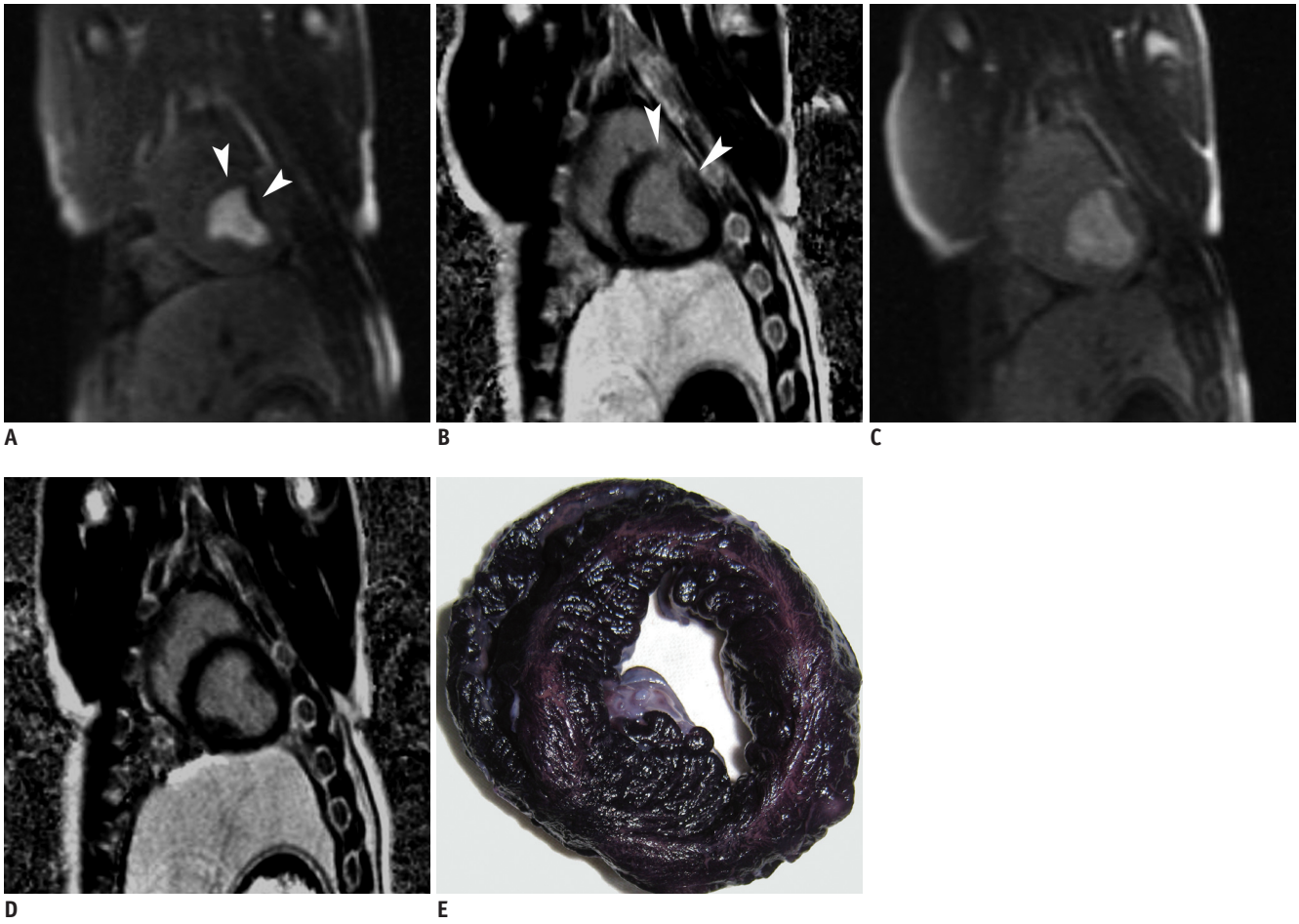

Fig. 2. Examples of MR perfusion, DE-MRI, and NBT staining in one animal.
First-pass perfusion **(A, C)** and DE-MRI **(B, D)** at 6 hours **(A, B)** and 1 week **(C, D)** demonstrate effects of microembolization induced by small-sized microemboli. Perfusion defect was visualized in embolized region at 6 hours (**A**, arrowheads) but largely decreased at 1 week after microembolization. DE-MRI demonstrated patchy hyperenhanced regions at 6 hours (**B**, arrowheads) but not at 1 week **(D)**. Microinfarcts were invisible to naked eye on NBT specimen **(E)** at 1 week after microembolization. DE-MRI = delayed contrast enhancement magnetic resonance imaging, NBT = nitrobluetetrazolium chloride

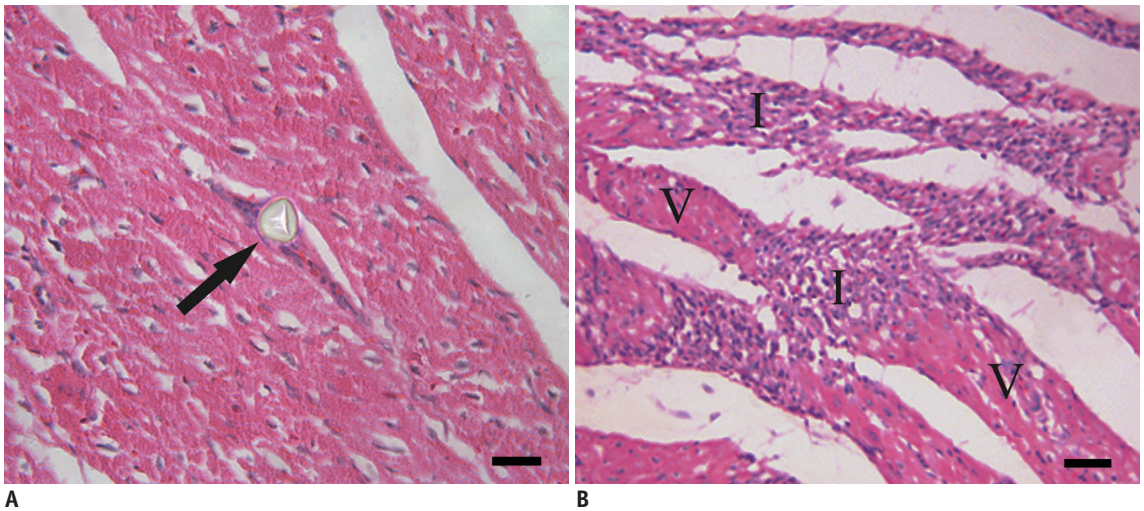

Fig. 3. Myocardial microinfarct demonstrated by microscopic examination.
Histologic slices (hematoxylin-eosin stain) obtained from target territory of coronary microembolization. Arrow **(A)** shows microsphere obstructing microvessel. I **(B)** indicates myocardial microinfarct and V **(B)** indicates viable myocardium. Scale bars = 50 μm.

of partial volume effects, and lower contrast material concentration in cases of incomplete myocardial necrosis. Importantly, delayed-enhancement is not specific for myocardial infarction. Contrast enhancement may occur in a variety of other disorders, such as tumor, myocarditis, and hypertrophic cardiomyopathy (31). The tumor necrosis factor-alpha (TNF-α)-mediated inflammatory response plays an important role in the myocardial damage following microembolization (9). Therefore, the inflammatory reactions as well as focal microinfarcts secondary to microembolization, which result in an increased distribution volume of MR contrast agents, could be the pathophysiologic mechanism for delayed-enhancement at 6 hours in the current study. The disappearance of hyperenhancement at 1 week can be attributed to the disappearance of interstitial edema accompanied by the decreased distribution volume of MR contrast agents (26, 32).

In magnitude image reconstruction, the performance of inversion recovery DE-MRI is highly sensitive to the choice of TI (31). Phase-sensitive reconstruction may reduce the variation in apparent size of hyperenhanced myocardium observed on magnitude images and render DE-MRI less sensitive to the choice of TI. Phase-sensitive reconstruction is also superior to magnitude reconstruction in terms of contrast-to-noise ratio, since phase-sensitive reconstruction can preserve the signal polarity and avoid decrease in contrast due to loss of polarity in magnitude images (28, 33). However, the background noise looks pixelated for phase-sensitive reconstruction because of the random phase and this may be a disadvantage.

Cine MRI showed a significant and persistent decline in the systolic wall thickening of the embolized region after microembolization in the current study. Our findings of persistent contractile dysfunction in the embolized region are generally in line with findings at 1 week and 7–8 weeks after embolization in pigs using larger embolic agents (21, 22). However, another study in dogs (32) using ultrasonic crystals embedded in the myocardium showed that profound contractile dysfunction occurred within hours after injection of small embolic agent (42 μm) and recovered spontaneously to basal values within 5–6 days after microembolization. The different responses to microembolization between studies may be attributed to the following factors: the size and number of the embolic agent used; the poor collateral circulation of humans and swines in comparison with that of dogs; and noninvasive vs. invasive approaches to acquire data. In the current study, the microvessel impairment is not expected to be severe, because of no grossly visible myocardial infarction and therefore, myocardial hibernation or stunning cannot be excluded (21). The persistent myocardial contractile dysfunction following microembolization may also be attributed to TNF-α-mediated inflammatory response, possible myocyte ongoing apoptosis, and progressive loss of cell integrity (9, 32, 34, 35).

Microvessel impairment could affect coronary circulation in patients with coronary artery disease, despite no visible obstruction in the conduit epicardial arteries at coronary angiography (2, 27, 36). This was also demonstrated in the current study using a swine model of coronary microembolization. Although normal-appearing epicardial arteries were observed immediately after the injection of microspheres, existing coronary microcirculation impairment could be detectable through MR perfusion imaging. Large decreases in the perfusion defect at the subacute stage may be attributed to the resorption of interstitial edema associated with microembolization and the complicated perfusion response to microembolic events. Experiments in the dog model (7, 37, 38) show that coronary blood flow undergoes a transient decrease immediately after microembolization, followed by a more prolonged increase, which is explained by release of adenosine from the patchy microembolized regions. Dörge et al. (7) suggest that a decrease of blood flow in microregions supplied by embolized microvessels is probably counterbalanced by reactive hyperemia in adjacent regions. However, species variation, such as the presence of extensive collateralization in dogs but not in humans or pigs may play an essential role in the different perfusion responses to microembolization.

There were some insufficiencies and limitations in our study. To our knowledge, an ideal animal model of spontaneous plaque rupture with subsequent microembolization does not exist currently. The microspheres used in this study were chemically inert and the pathophysiological effect may differ from that of plaque and thrombus microembolization in patients. Therefore, the swine model used in this study could only partly mimic the *in vivo* situation of coronary microembolization; in addition, the current study was only designed to assess the acute and subacute effect of defined size and load of coronary small-sized microemboli. Another limitation is that pathological analysis was only performed at 1 week but not at 6 hours after microembolization.

Korean Journal of Radiology
KJR

In conclusion, coronary microembolization induced by a certain load of small-sized microemboli may cause normal-appearing epicardial coronary arteries on catheter coronary angiography and result in myocardial infarcts invisible to the naked eye. MRI characterization of myocardial impairments due to such microembolization includes the decline in myocardial dysfunction and perfusion at cine and first-pass perfusion imaging, and transient hyperenhancement at DE-MRI. Regional evaluation of myocardial contractility and perfusion by cine and first-pass perfusion MRI may be better than DE-MRI for evaluating the ischemic cascade due to coronary microembolization. It has potential clinical benefit in explaining the mismatch between epicardial arterial blood flow and myocardial dysfunction, and follow-up examinations.

REFERENCES

1. Porto I, Selvanayagam JB, Van Gaal WJ, Prati F, Cheng A, Channon K, et al. Plaque volume and occurrence and location of periprocedural myocardial necrosis after percutaneous coronary intervention: insights from delayed-enhancement magnetic resonance imaging, thrombolysis in myocardial infarction myocardial perfusion grade analysis, and intravascular ultrasound. *Circulation* 2006;114:662-669
2. Baumgart D, Liu F, Haude M, Görge G, Ge J, Erbel R. Acute plaque rupture and myocardial stunning in patient with normal coronary arteriography. *Lancet* 1995;346:193-194
3. Falk E. Unstable angina with fatal outcome: dynamic coronary thrombosis leading to infarction and/or sudden death. Autopsy evidence of recurrent mural thrombosis with peripheral embolization culminating in total vascular occlusion. *Circulation* 1985;71:699-708
4. Kotani J, Nanto S, Mintz GS, Kitakaze M, Ohara T, Morozumi T, et al. Plaque gruel of atheromatous coronary lesion may contribute to the no-reflow phenomenon in patients with acute coronary syndrome. *Circulation* 2002;106:1672-1677
5. Henriques JP, Zijlstra F, Ottervanger JP, de Boer MJ, van't Hof AW, Hoorntje JC, et al. Incidence and clinical significance of distal embolization during primary angioplasty for acute myocardial infarction. *Eur Heart J* 2002;23:1112-1117
6. Selvanayagam JB, Cheng AS, Jerosch-Herold M, Rahimi K, Porto I, van Gaal W, et al. Effect of distal embolization on myocardial perfusion reserve after percutaneous coronary intervention: a quantitative magnetic resonance perfusion study. *Circulation* 2007;116:1458-1464
7. Dörge H, Neumann T, Behrends M, Skyschally A, Schulz R, Kasper C, et al. Perfusion-contraction mismatch with coronary microvascular obstruction: role of inflammation. *Am J Physiol Heart Circ Physiol* 2000;279:H2587-H2592
8. Topol EJ, Yadav JS. Recognition of the importance of embolization in atherosclerotic vascular disease. *Circulation* 2000;101:570-580
9. Skyschally A, Leineweber K, Gres P, Haude M, Erbel R, Heusch G. Coronary microembolization. *Basic Res Cardiol* 2006;101:373-382
10. Jeremy RW, Links JM, Becker LC. Progressive failure of coronary flow during reperfusion of myocardial infarction: documentation of the no reflow phenomenon with positron emission tomography. *J Am Coll Cardiol* 1990;16:695-704
11. Asanuma T, Tanabe K, Ochiai K, Yoshitomi H, Nakamura K, Murakami Y, et al. Relationship between progressive microvascular damage and intramyocardial hemorrhage in patients with reperfused anterior myocardial infarction: myocardial contrast echocardiographic study. *Circulation* 1997;96:448-453
12. Gerber BL, Rochitte CE, Melin JA, McVeigh ER, Bluemke DA, Wu KC, et al. Microvascular obstruction and left ventricular remodeling early after acute myocardial infarction. *Circulation* 2000;101:2734-2741
13. Kaul S, Ito H. Microvasculature in acute myocardial ischemia: part II: evolving concepts in pathophysiology, diagnosis, and treatment. *Circulation* 2004;109:310-315
14. Litchfield RL. Noninvasive tests for cardiac risk stratification. Which ones are most prognostic? *Postgrad Med* 2004;115:30-36
15. Poon M, Fuster V, Fayad Z. Cardiac magnetic resonance imaging: a "one-stop-shop" evaluation of myocardial dysfunction. *Curr Opin Cardiol* 2002;17:663-670
16. Finn JP, Nael K, Deshpande V, Ratib O, Laub G. Cardiac MR imaging: state of the technology. *Radiology* 2006;241:338-354
17. Sakuma H, Ichikawa Y, Suzawa N, Hirano T, Makino K, Koyama N, et al. Assessment of coronary arteries with total study time of less than 30 minutes by using whole-heart coronary MR angiography. *Radiology* 2005;237:316-321
18. Jin H, Zeng MS, Ge MY, Ma JY, Chen CZ, Shen JZ, et al. Influence of applying nitroglycerin in whole-heart free-breathing 3D coronary MR angiography. *AJR Am J Roentgenol* 2010;194:927-932
19. Yun H, Zeng MS, Jin H, Yang S. Isolated noncompaction of ventricular myocardium: a magnetic resonance imaging study of 11 patients. *Korean J Radiol* 2011;12:686-692
20. Carlsson M, Wilson M, Martin AJ, Saeed M. Myocardial microinfarction after coronary microembolization in swine: MR imaging characterization. *Radiology* 2009;250:703-713
21. Carlsson M, Martin AJ, Ursell PC, Saloner D, Saeed M. Magnetic resonance imaging quantification of left ventricular dysfunction following coronary microembolization. *Magn Reson Med* 2009;61:595-602
22. Carlsson M, Jablonowski R, Martin AJ, Ursell PC, Saeed M. Coronary microembolization causes long-term detrimental effects on regional left ventricular function. *Scand Cardiovasc J* 2011;45:205-214
23. Carlsson M, Saloner D, Martin AJ, Ursell PC, Saeed M. Heterogeneous microinfarcts caused by coronary microemboli: evaluation with multidetector CT and MR

imaging in a swine model. *Radiology* 2010;254:718-728
24. Möhlenkamp S, Beighley PE, Pfeifer EA, Behrenbeck TR, Sheedy PF 2nd, Ritman EL. Intramyocardial blood volume, perfusion and transit time in response to embolization of different sized microvessels. *Cardiovasc Res* 2003;57:843-852
25. Saeed M, Hetts SW, Do L, Sullivan SM, Wilson MW. MRI quantification of left ventricular function in microinfarct versus large infarct in swine model. *Int J Cardiovasc Imaging* 2013;29:159-168
26. Breuckmann F, Nassenstein K, Bucher C, Konietzka I, Kaiser G, Konorza T, et al. Systematic analysis of functional and structural changes after coronary microembolization: a cardiac magnetic resonance imaging study. *JACC Cardiovasc Imaging* 2009;2:121-130
27. Rodrigues de Avila LF, Fernandes JL, Rochitte CE, Cerri GG, Filho JP. Perfusion impairment in patients with normal-appearing coronary arteries: identification with contrast-enhanced MR imaging. *Radiology* 2006;238:464-472
28. Kellman P, Arai AE, McVeigh ER, Aletras AH. Phase-sensitive inversion recovery for detecting myocardial infarction using gadolinium-delayed hyperenhancement. *Magn Reson Med* 2002;47:372-383
29. Heiberg E, Sjögren J, Ugander M, Carlsson M, Engblom H, Arheden H. Design and validation of Segment--freely available software for cardiovascular image analysis. *BMC Med Imaging* 2010;10:1
30. Landis JR, Koch GG. The measurement of observer agreement for categorical data. *Biometrics* 1977;33:159-174
31. Edelman RR. Contrast-enhanced MR imaging of the heart: overview of the literature. *Radiology* 2004;232:653-668
32. Skyschally A, Haude M, Dörge H, Thielmann M, Duschin A, van de Sand A, et al. Glucocorticoid treatment prevents progressive myocardial dysfunction resulting from experimental coronary microembolization. *Circulation* 2004;109:2337-2342
33. Huber AM, Schoenberg SO, Hayes C, Spannagl B, Engelmann MG, Franz WM, et al. Phase-sensitive inversion-recovery MR imaging in the detection of myocardial infarction. *Radiology* 2005;237:854-860
34. Jiang L, Huang Y, Hunyor S, dos Remedios CG. Cardiomyocyte apoptosis is associated with increased wall stress in chronic failing left ventricle. *Eur Heart J* 2003;24:742-751
35. Chen ZW, Qian JY, Ma JY, Chang SF, Yun H, Jin H, et al. TNF-α-induced cardiomyocyte apoptosis contributes to cardiac dysfunction after coronary microembolization in mini-pigs. *J Cell Mol Med* 2014;18:1953-1963
36. De Bruyne B, Hersbach F, Pijls NH, Bartunek J, Bech JW, Heyndrickx GR, et al. Abnormal epicardial coronary resistance in patients with diffuse atherosclerosis but "Normal" coronary angiography. *Circulation* 2001;104:2401-2406
37. West JW, Kobayashi T, Anderson FS. Effects of selective coronary embolization on coronary blood flow and coronary sinus venous blood oxygen saturation in dogs. *Circ Res* 1962;10:722-738
38. Hori M, Inoue M, Kitakaze M, Koretsune Y, Iwai K, Tamai J, et al. Role of adenosine in hyperemic response of coronary blood flow in microembolization. *Am J Physiol* 1986;250(3 Pt 2):H509-H518